NASA Technical Memorandum 103839

Computations of Unsteady Multistage Compressor Flows in a Workstation Environment

Karen L. Gundy-Burlet

June 1992

NASA

National Aeronautics and
Space Administration

SUMMARY

High-end graphics workstations are becoming a necessary tool in the computational fluid dynamics environment. In addition to their graphics capabilities, workstations of the latest generation have powerful floating-point-operation capabilities. As workstations become common, they could provide valuable computing time for such applications as turbomachinery flow calculations. This report discusses the issues involved in implementing an unsteady, viscous multistage-turbomachinery code (STAGE-2) on workstations. It then describes work in which the workstation version of STAGE-2 was used to study the effects of axial-gap spacing on the time-averaged and unsteady flow within a $2\frac{1}{2}$-stage compressor. The results include time-averaged surface pressures, time-averaged pressure contours, standard deviation of pressure contours, pressure amplitudes, and force polar plots.

NOMENCLATURE

C_p pressure coefficient, $C_p = \dfrac{P - P_{T_i}}{(1/2)\rho_i U_m^2}$

F airfoil force per unit span normalized by Q_{U_m} and τ

n number of timesteps per cycle

P pressure

$\overline{P}$ time-averaged pressure

P' standard deviation of pressure

P_{T_i} compressor inlet total pressure

Q_{U_m} dynamic pressure based on U_m

U_m wheel speed at midspan

x axial distance

ρ density

τ airfoil pitch

Subscripts

i inlet

t tangential component

x axial component

INTRODUCTION

Flows in turbomachines are difficult to analyze because of the time-varying geometries and inherently unsteady flow. Experimental techniques exist to investigate the time-averaged and unsteady flow within turbomachines, but they can be expensive to use. Because of this, analytical techniques have been used to supplement the knowledge gained from experimentation. As computer resources became available, computational techniques were also used to supplement knowledge of turbomachinery flows. In these earlier works, various levels of approximation were applied to make turbomachinery flow computations tractable on the available computers. Unfortunately, these approximations also restricted the usefulness of the computational model and the information it generated. Only recently have two- and three-dimensional unsteady viscous-flow computations been possible; however, these unsteady analyses have been considered impractical for routine design purposes because of their memory usage, run times, and dependence on supercomputer technology. Improvements in computer technology are rapidly making these computations practical on a range of computers from supercomputers to single-user workstations.

Supercomputers are expensive to buy, maintain, and upgrade. Because of this, they tend not to be replaced or upgraded until they are seriously overutilized. This leads to long job queues and slow turnaround times on jobs. Raw computer speed is irrelevant if jobs are unable to get through the system in a reasonable amount of time. To the researcher, the wall-clock time is often more critical than the cpu time required for convergence.

Even on an unloaded supercomputer, job accounting procedures can limit the amount of cpu time available to an individual. Typically, an individual is allocated a certain amount of time or is charged for time used. In either case, supercomputer cpu usage has to be carefully budgeted, and other sources of cpu time must be found. A reasonable compromise to these constraints has been provided by the latest generation of workstations. A dedicated workstation can provide wall-clock time performance on the order of that of a heavily loaded supercomputer at a comparatively low cost to the researcher. This report discusses the issues involved in implementing a two-dimensional, unsteady, viscous, multistage turbomachinery code (STAGE-2) on workstations.

Results from STAGE-2 were compared with experimental data for a single-stage turbine and a $2\frac{1}{2}$-stage compressor in Gundy-Burlet, Rai, and Dring

(1989) and Gundy-Burlet et al. (1990). In the current study, STAGE-2 was used to examine the effect of axial gap on the unsteady flow in a $2\frac{1}{2}$-stage compressor. The axial gaps used in this study were 20%, 35%, and 50% of the average axial chord in the compressor. The time average and standard deviation of the pressure field were used to investigate steady and unsteady flow features. In addition, surface pressures and force polar plots were examined. Coarse-grid results were obtained on workstations; fine-grid results were obtained on both supercomputers and workstations.

The author would like to thank Marcel Burlet, Dan Magenheimer, and Tim Bailey of Hewlett-Packard for their help in obtaining timings on Hewlett-Packard workstations. In addition, the author would like to thank Dr. A. Sugavanam, Sundar Raman, and Gwen Swan of IBM for providing both timings and computational time on IBM workstations.

ALGORITHM

The current work is based on an extension of an approach developed by Rai and the approach is discussed in detail in Rai (1987) and Rai and Madavan (1990). The approach is reviewed in brief here. The flow field is divided into two basic types of zones. Inner "O" grids are used to resolve the flow field near the airfoils. These "O" grids are overlaid on outer "H" grids, which are used to resolve the flow field in the passages between airfoils. The "H" grids are allowed to slip relative to one another to simulate the relative motion between rotors and stators. Thin-layer Navier-Stokes equations are solved in the inner zones, where viscous effects are important, and Euler equations are used in the outer zones, where viscous effects are weak. The governing equations are cast in the strong conservation form. A fully implicit finite-difference method is used to advance the solution of the governing equations in time, and a Newton-Raphson subiteration scheme is used to reduce the linearization and factorization errors at each time step. The convective terms are evaluated using a third-order-accurate upwind-biased Roe scheme, and the viscous terms are evaluated using second-order-accurate central differences. The Baldwin-Lomax (1978) turbulence model is used to compute the turbulent eddy viscosity. Details of the turbulence model, zonal and natural boundary conditions, grid configuration, book-

keeping system, and database management systems are discussed in Gundy-Burlet, Rai, and Dring (1989).

COMPUTER ARCHITECTURE ISSUES

Efficient implementation of a computer code requires knowledge of the computer on which it will operate. There are several basic differences between the architectures of supercomputers and workstations that require implementation changes in the code. One major difference between supercomputers and workstations is the size of their main memories. For instance, the NASA Ames CRAY-2 has an internal memory of 2 Gbytes, and a typical workstation has between 8 Mbytes and 64 Mbytes of memory. Extended memory, such as disk or Solid State Disk (SSD), is also available on a supercomputer. Virtual-memory workstations can also access disk when main memory is used up.

The speed of transfer of information between main memory and extended memory is another major difference between workstations and supercomputers. Supercomputers have high-bandwidth channels between main memory and disk or SSD that provide fast input/output (I/O). Software support for unblocked, random-access I/O is also usually provided in FORTRAN on supercomputers. This is an efficient mechanism to output data to disk or SSD. Workstations do not support high-bandwidth channels between main memory and disk. If the disk is used to supplement main memory on a virtual-memory machine, the "swapping" of data between disk and main memory can be extremely slow. In addition, it is difficult to perform efficient I/O from FORTRAN on a workstation.

A third difference between workstations and the CRAY in particular is that the CRAY is a vector processor and the workstation is a scalar processor. The large memory combined with the vector capabilities of the CRAY provides the opportunity to trade memory usage for speed. For instance, although block tridiagonal inversions have data dependencies that inhibit vectorization, they can be vectorized by processing several inversions simultaneously. This requires additional memory usage to store the block elements for each inversion, but can dramatically accelerate a code. Since current workstations are scalar processors, this vectorization strategy would not speed up the code on a workstation. If the additional memory usage required that

virtual memory (disk) be accessed, the wall-clock time used could actually increase by an order of magnitude.

With these factors in mind, the workstation version of the STAGE-2 code was designed to store data in internal buffer arrays. These arrays are efficiently packed to reduce memory usage and to minimize or eliminate the use of virtual memory. In addition, many arrays that are used to enhance vector processing are eliminated in the workstation version of the code. Approximately 120 bytes of memory are required per grid point for the workstation version of STAGE-2.

GEOMETRY AND GRID

The $2\frac{1}{2}$-stage compressor geometry used in this study models the midspan geometry of an experiment that is part of the AGARD (1989) collection of test cases for computations of internal flows in aero-engine components. Much of the data for this compressor is also tabulated in Dring and Joslyn (1985). The experimental configuration consists of an inlet guide vane followed by two rotor/stator pairs. There are 44 airfoils in each row, leading to a 1:1 ratio of airfoils from row to row down the compressor. As it would be prohibitively expensive to compute the flow through the entire 220-airfoil system, the flow is computed through only one passage, and periodicity is used to model the other 43 passages. The axial gaps between airfoil rows in the experimental configuration are approximately 50% of the average axial chord. In this study the flow through the compressor is computed with the same midspan airfoil geometry, but with varying axial gaps.

In Gundy-Burlet, Rai, and Dring (1989) and Gundy-Burlet et al. (1990), a parabolic-arc inlet guide vane was used because the actual vane geometry was unavailable. The vane geometry has recently become available and is used in the current calculation. The first and second stages of the compressor are similar, except that the first-stage rotor is closed 3° from axial relative to the second-stage rotor. This reduces the angle of attack of the first-stage rotor. The airfoil sections are all defined by NACA 65–series airfoils imposed on a circular-arc mean camber line. The average chord is 4 in.

A zonal grid system is used to discretize the flow field within the $2\frac{1}{2}$-stage compressor. Figure 1 shows the zonal grid system used for the 20%-gap case. For clarity in figure 1, every other point in the grid has been plotted. There are two grids associated with each

airfoil: an inner, body-centered "O" grid and an outer, sheared, Cartesian "H" grid. The thin-layer Navier-Stokes equations are solved on the inner grids, whose grid points are clustered near the airfoil to resolve the viscous terms, and the Euler equations are solved on the outer grids. The rotor and stator grids are allowed to slip past each other to simulate the relative motion between rotor and stator airfoils. In addition to the two grids used for each airfoil, there are an inlet and an exit grid, thus yielding a total of 12 grids.

In order to generate inner grids that are wholly contained by the outer grids but not distorted, it is necessary to overlap the rotor and stator outer grids in the gap regions for the 20%-axial-gap case. This can be seen in the 20%-axial-gap grid shown in figure 1. This required a modification of the grid generator and algorithm, and permited study of turbomachines with small axial gaps.

Coarse grids are used to validate workstation results. The inner grids are dimensioned 151×31. The outer grids have a varying number of points in the axial direction, but they all have 61 points in the circumferential direction. The inlet and outlet grids have 28 and 30 points in the axial direction, respectively. The outer grids associated with an airfoil average 77 points in the axial direction. This leads to a total of 50,367 points for all zones in the coarse-grid configuration.

Fine grids are used to obtain detailed data regarding the steady and unsteady flow structure in the compressor. The inner grids are dimensioned 214×44. The outer grids have a varying number of points in the axial direction because of the change in axial gap and axial extent of each airfoil, but they all have 87 points in the circumferential direction. The inlet and outlet grids have 40 and 42 points in the axial direction, respectively. The outer grids associated with an airfoil average 99 points in the axial direction for the 20%-gap case, 101 points for the 35%-gap case, and 110 points for the 50%-gap case. This leads to a total of 97,279 points for all zones in the fine-grid configuration for the 20%-gap case, 98,323 points for the 35%-gap case, and 102,064 points for the 50%-gap case.

RESULTS

The results reported in this section are for the $2\frac{1}{2}$-stage compressor described above. These results were all computed at an inlet Mach number of 0.07,

3

an inlet Reynolds number of 100,000 per in., and a pressure rise of $C_p = 1.11$. Several approximations should be considered when interpreting the following results. The flow in the compressor is three-dimensional with end-wall boundary layer growth, hub corner stall, and tip leakage effects. Because STAGE-2 is a two-dimensional code, it is unable to compute these three-dimensional effects. Stream-tube contraction terms have not been implemented in the code, so the effect of the end-wall boundary layer growth is not modeled.

For the coarse-grid computation, 2 subiterations per time step and 500 time steps per cycle are sufficient to provide stability and yet eliminate transients from the solution. A cycle is defined as the time it takes a rotor to move from its position relative to one stator to the corresponding position relative to the next stator. The code was benchmarked on several different workstations for a 50,367-point grid and for 2 subiterations per time step. Five hundred time steps per cycle and 2 subiterations per time step were found to be sufficient for converging this coarse-grid $2\frac{1}{2}$-stage-compressor calculation. Table 1 gives the code's performance on several workstations, which range in price from $10,000 to $100,000. It is not the purpose of this study to present price/performance comparisons between different workstations. Instead, it is meant to show that STAGE-2 will operate on a wide variety of workstations and to give a general idea of its performance on these workstations. The performance is measured both by cpu time per iteration per grid point (cpu/it/pt) and by the MFLOP rate. The MFLOP rate for the workstations was computed by determining the number of floating-point operations in a run using a profiler on a CRAY-YMP. The number of floating-point operations is assumed to be the same for the workstations, and is divided by the cpu time to get an overall MFLOP rate.

Timings for the CRAY-YMP are included in table 1 to provide comparisons between supercomputer rates and workstation rates. All the timings reported here are for single-processor hours. The timings on the CRAY-YMP illustrate the benefits of using additional memory to enhance vectorization. The overall cpu time of the code is decreased by a factor of 2.3 if additional memory is used to perform several inversions at once in the block tridiagonal solver. The vectorization in the block tridiagonal solver is the only difference between the scalar and vector versions of the code in this study. The scalar version of STAGE-2 runs

at 2.0 MFLOPS on even the least expensive workstation used. With 2 subiterations per time step, 500 time steps per cycle, and a 50,367-point grid, this translates to a turnaround time of 16 clock hours for one cycle on a dedicated low-end machine. For the fastest workstation used in this study, a cycle can be obtained in less than 2.6 clock hours. With the continuing rapid improvement in workstation technology, these timings will improve dramatically in the near future.

One concern when implementing a computational fluid dynamics (CFD) code on a workstation is the effect of word length on the accuracy of the solution. The CRAY-class supercomputers have a 64-bit word length, and the workstations used in this study have a 32-bit word length. To address this issue, a coarse-grid calculation using the experimental axial gap spacing was performed. Workstation-generated time-averaged surface pressures are compared with experimental data in figure 2. The time-averaged pressures are obtained by averaging the instantaneous static pressure over one cycle. The pressures are then nondimensionalized and plotted with respect to axial distance. The workstation results compare well with the experimental data and are nearly identical to the supercomputer results. This indicates that the 32-bit word length on the workstation is sufficient to generate accurate solutions.

Time-averaged pressure contours are presented in figure 3 and standard deviation of pressure contours in figure 4 for the field around the second-stage rotor for three different axial gaps. In these figures, the pressure is averaged in the rotor frame of reference. The standard deviation is also computed in the rotating frame of reference for the second-stage rotor. The standard deviation of the pressure field at each point is computed as

$$P' = \sqrt{\frac{\sum_{i=1}^{n}(P_i - \bar{P})^2}{n-1}}$$

where n is the number of time steps in a cycle. Darker shades indicate higher pressures or higher levels of unsteadiness. The locus of points described by the the trailing edge of the first-stage stator and the leading edge of the second-stage stator are plotted as dashed lines. The time-averaged flow fields are qualitatively similar for the different axial gap cases. Contours of P' show that the greatest unsteadiness is near the leading edge of the stator. This is most pronounced for the 20%-axial-gap case (fig. 4(a)).

Time-averaged pressure contours and standard deviation of pressure contours are presented in figures 5

Table 1. STAGE-2 performance statistics

Machine	Memory	cpu/it/pt	MFLOPS
CRAY-YMP[a]	128 Mwords	81.4 μsec	58
CRAY-YMP[b]	128 Mwords	35.7 μsec	131
HP 9000/835	16 Mbytes	2.34 msec	2.0
HP 9000/720	16 Mbytes	0.37 msec	12.9
IBM 6000/530	48 Mbytes	0.50 msec	9.6
SGI 4D25	16 Mbytes	1.57 msec	3.0
SGI 4D210GTX	32 Mbytes	1.24 msec	3.8
SGI 4D320VGX	48 Mbytes	0.95 msec	5.0

[a]STAGE-2 scalar version.
[b]STAGE-2 vector version.

and 6, respectively, for the second-stage stator. The time-averaged pressures and standard deviation are computed in the stator frame of reference. The locus of points described by the trailing edge of the second-stage rotor is plotted in this figure as a dashed line. The time-averaged field pressures for the 20%, 35%, and 50% cases are similar to one another. The 20%-gap case (fig. 6(a)) shows a higher level of unsteadiness near the second-stage rotor trailing-edge locus than in the rest of the field. The area immediately surrounding the leading edges of the second-stage stator are also more unsteady than the rest of the field, for each of the axial gaps.

Figures 3-6 give a qualitative view of the steady and unsteady flow features in the second stage of the compressor. As can be surmised from these figures, the time-averaged surface pressures for the three axial gaps are similar to each other. They also closely resemble those for the experimental gap configuration in figure 2, and hence are not reported here. The surface-pressure amplitudes do vary with axial gap; they are shown in figure 7 for each airfoil in the compressor. The pressure amplitudes are computed by determining the maximum and minimum pressure at each point on the surface over a cycle and then subtracting the minimum pressure from the maximum pressure. As expected, the 20%-gap case (fig. 7(a)) shows the greatest level of unsteadiness, and the 35%-gap case (fig. 7(b)) generally shows more unsteadiness than the 50%-gap case (fig. 7(c)). Because the airfoils are farther apart in the 35%- and 50%-gap cases, the effect of the potential fields is reduced. This reduces the overall level of unsteadiness of pressure in the compressor.

Pressure-amplitude plots yield information regarding the level of unsteadiness in the compressor, but do not contain phase information. Force polar plots are used to investigate both the frequencies and the amplitudes associated with the unsteadiness. In figures 8 and 9, force polar plots are presented for the second stage of the compressor for all three axial gap cases. These plots are generated by integrating the instantaneous surface-pressure field and resolving the resultant force into its axial and tangential components. The tangential force is then plotted against the axial force. For a periodic solution, this curve should close on itself at the end of a cycle, and is a good measure of the convergence of a solution to a periodic state. Figure 7 shows that the overall unsteadiness in the compressor increases as axial gap decreases. However, the integrated force field does not necessarily become more unsteady as the axial gap decreases. The force polar for the second-stage rotor at an axial gap of 20% (fig. 8(a)) shows more unsteadiness than either the 35%-axial-gap case (fig. 8(b)) or the 50%-axial-gap case. However, the integrated forces are more unsteady for the 50%-axial-gap case than for the 35%-axial-gap case. Animations of these flows indicate that for the 50%-gap case, the second-stage rotor interacts with wakes that interacted with each other. This reduces the frequency with which the rotor passes through upstream wakes, but increases the amplitude of the force polar. For the 35%-gap case, the wakes from upstream airfoils are encountered at different times, so the frequency of the force variation is higher, but the amplitude is reduced.

A similar effect is seen in figure 9 for the forces on the second-stage stator. The amplitude of the forces is smallest for the 20%-gap case (fig. 9(a)) and largest for the 50%-gap case (fig. 9(c)). Note that the passage of each individual wake can be seen in the force polar for the 35%-gap case. The IGV wake is seen as the smallest amplitude loop (on the left). The farther downstream the wake is generated, the larger the

amplitude of the loop. Despite the fact that the un-steadiness of the pressure field increases as the axial gap decreases, the actual force amplitude on the airfoil may decrease.

CONCLUSIONS

A third-order-accurate upwind-biased thin-layer Navier-Stokes zonal code (STAGE-2) was used to investigate the flow within a multistage compressor. It was shown that STAGE-2 can be used to compute unsteady, multistage-compressor flows in a workstation environment. The rapid development of workstation technology has and will make possible the regular use of workstations as valuable sources of computational time. In the future, STAGE-2 will be used in a networked workstation environment to investigate distributed processing of unsteady turbomachinery flows. This will further increase the value of workstation networks as a source of computational time.

The effects of axial gap spacing on the unsteady flow within a $2\frac{1}{2}$-stage compressor were investigated. As the axial gap is reduced, the potential interaction between airfoils becomes more significant. However, the wake-interaction effects can vary with axial gap depending on the relative phase between the wakes. The force amplitude can be smaller even though the gap has been decreased. It is surmised that airfoil phase must be considered in estimating interaction effects.

REFERENCES

AGARD: 1989. Test Cases for Computation of Internal Flows in Aero Engine Components. AGARD Propulsion and Energetics Panel, Working Group 18, AGARD-AR-275.

Baldwin, B. S.; and Lomax, H.: 1978. Thin Layer Approximation and Algebraic Model for Separated Turbulent Flow. AIAA Paper 78-257, Jan.

Dring, R. P.; and Joslyn, H. D.: 1985. An Assessment of Single- and Multi-Stage Compressor Flow Modeling. Final Report for Naval Air Systems Command Contract No. N00014-84-C-0354, July, AD-B102 101.

Gundy-Burlet, K. L.; Rai, M. M.; and Dring, R. P.: 1989. Two-Dimensional Computations of Multistage Compressor Flows Using a Zonal Approach. AIAA Paper 89-2452, July.

Gundy-Burlet, K. L.; Rai, M. M.; Stauter, R. C.; and Dring, R. P.: 1990. Temporally and Spatially Resolved Flow in a Two-Stage Axial Compressor. ASME Paper 90-GT-299, June.

Rai, M. M.: 1987. Navier-Stokes Simulations of Rotor/Stator Interactions Using Patched and Overlaid Grids. J. Propulsion Power, vol. 3, no. 5, pp. 387-396.

Rai, M. M.; and Madavan, N. K.: 1990. Multi-Airfoil Navier-Stokes Simulations of Turbine Rotor-Stator Interaction. J. Turbomachinery, vol. 112, July, pp. 337-384.
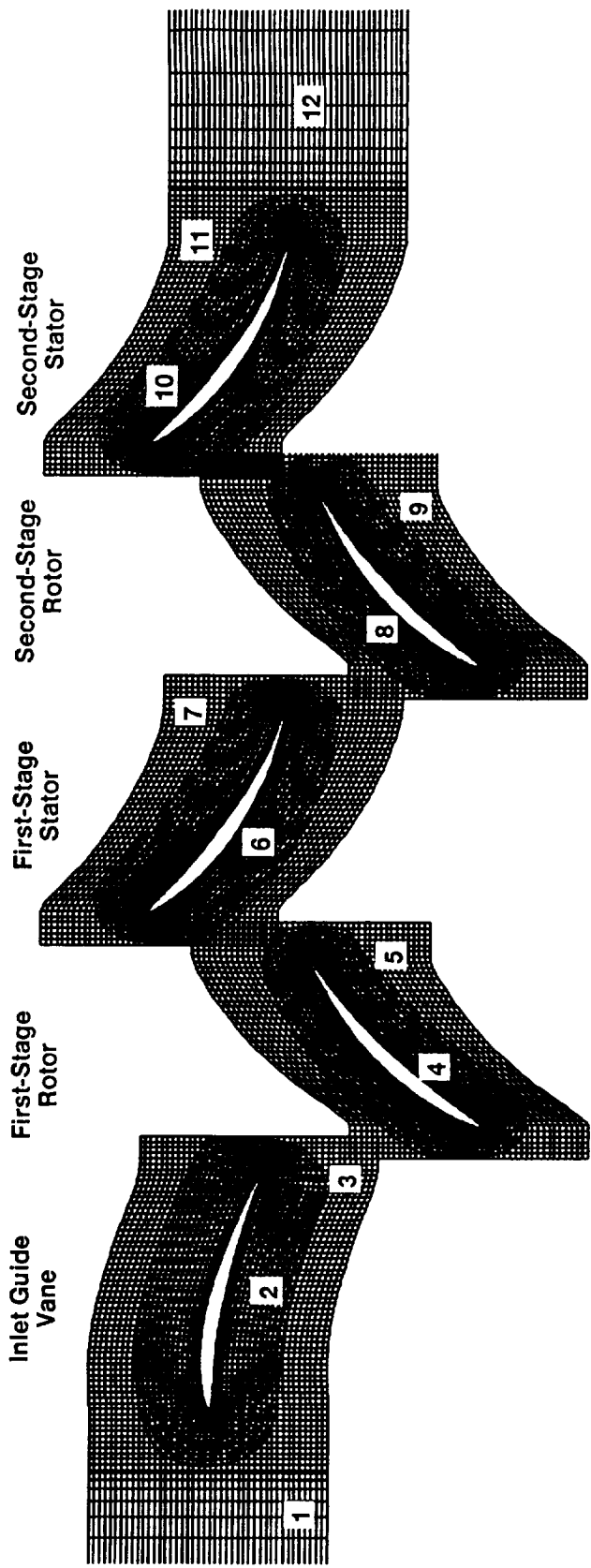
Figure 1. Zonal grid topology.
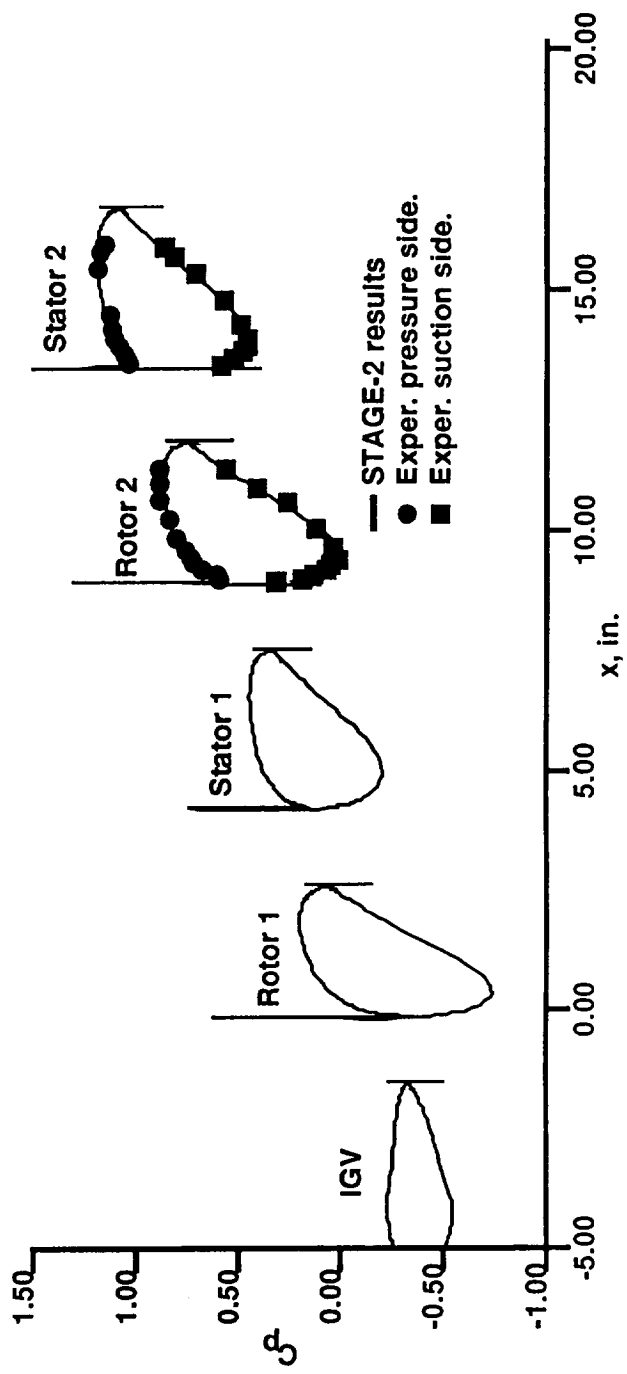
Figure 2. Time-averaged surface pressures, experimental gap configuration.
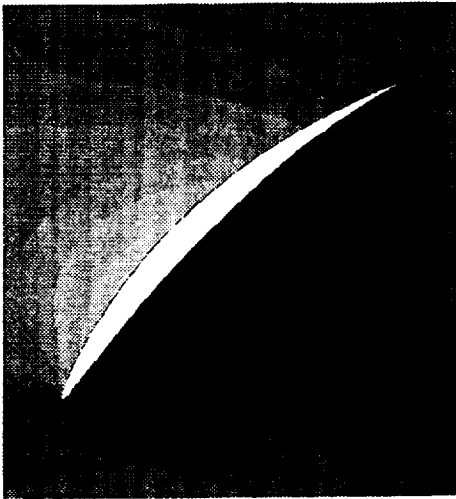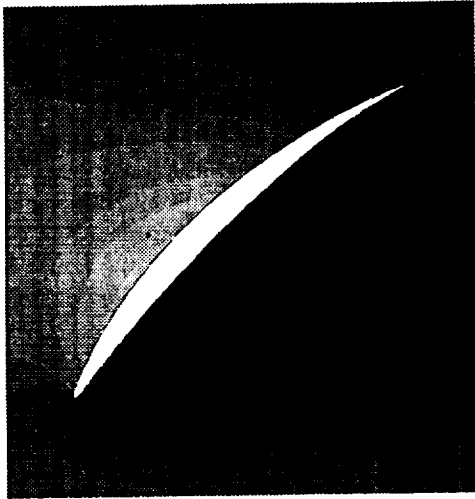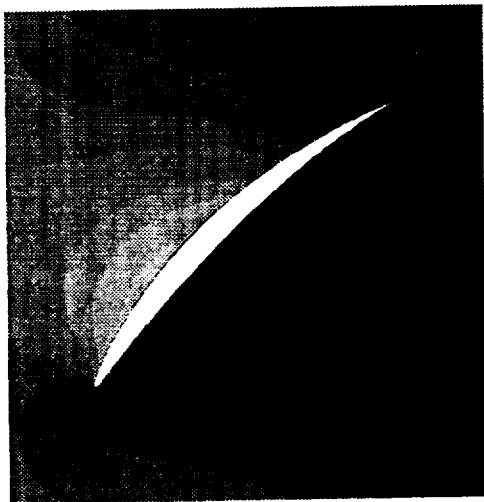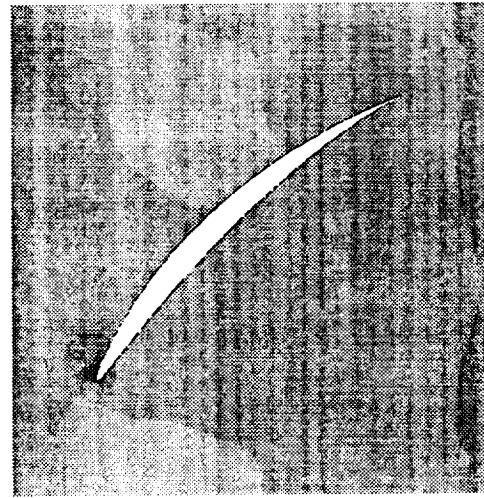
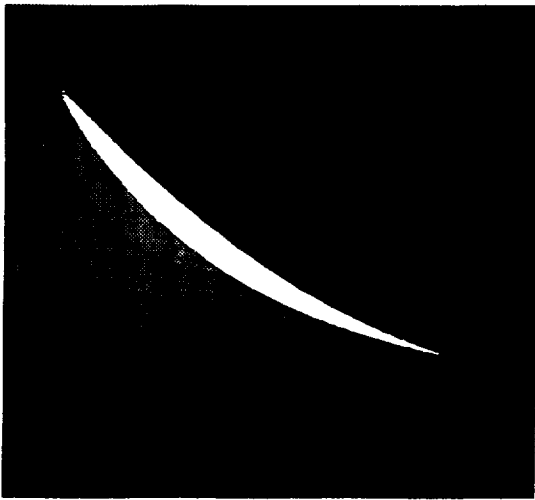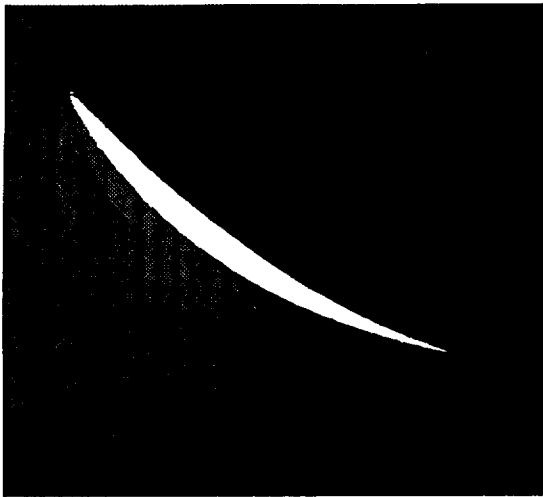Figure 3. Second-stage-rotor time-averaged pressure contours. (a) 20% gap, (b) 35% gap, (c) 50% gap.
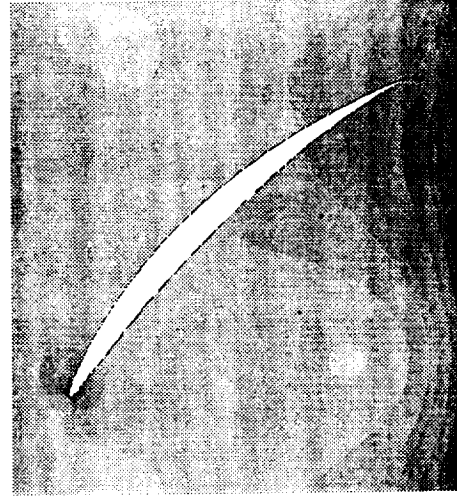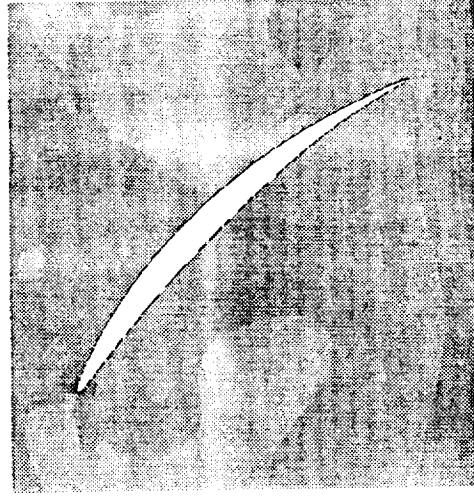
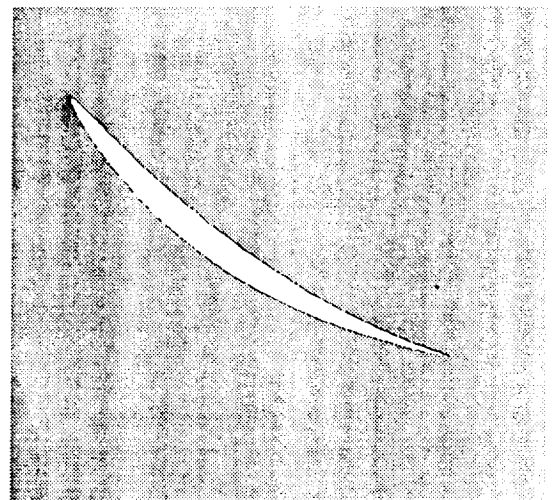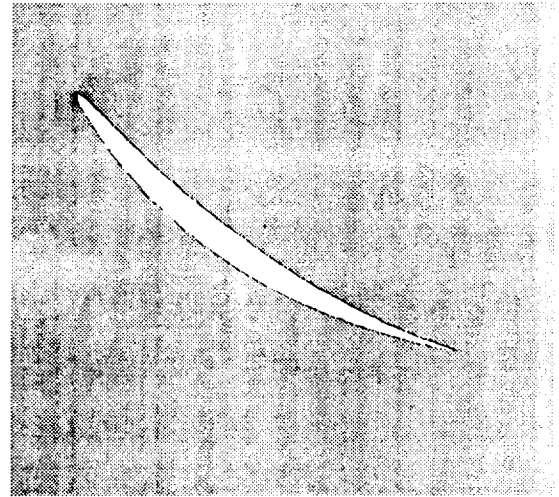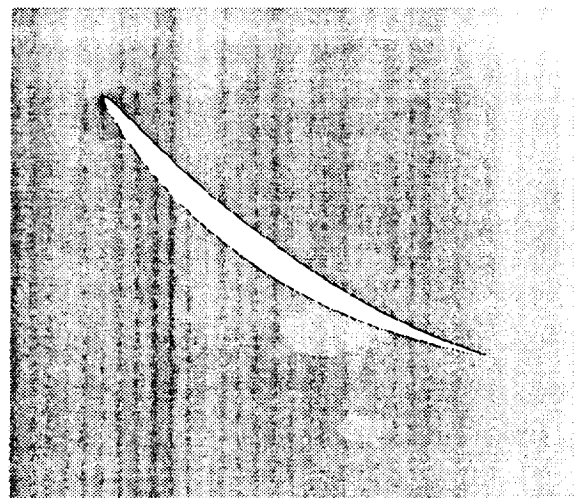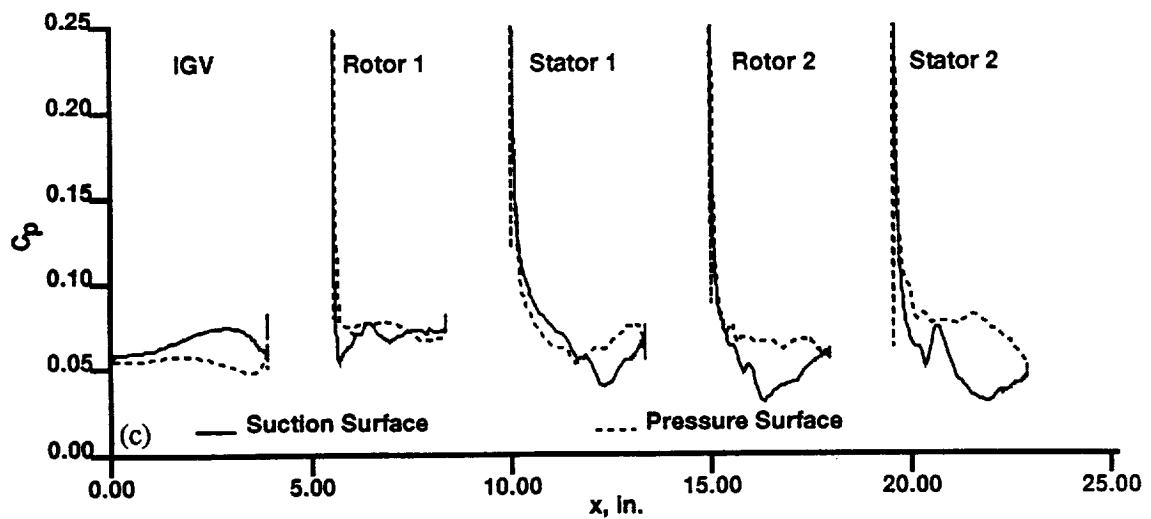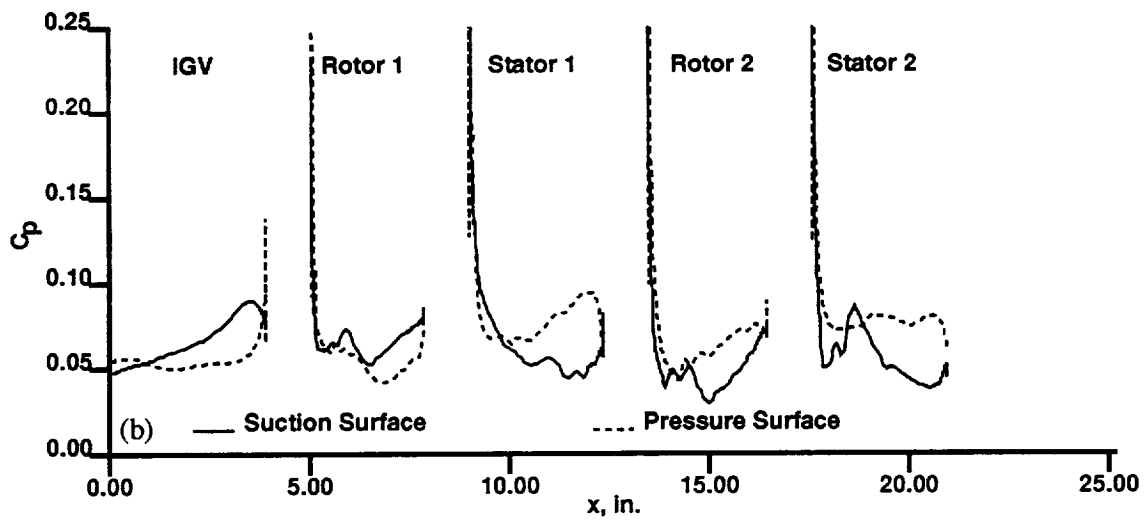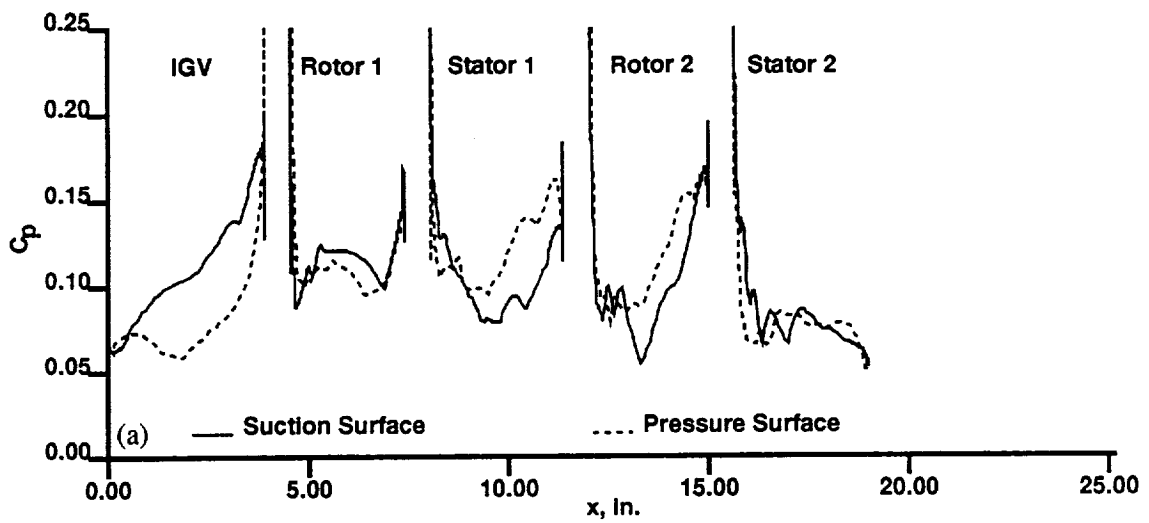Figure 4. Second-stage-rotor standard-deviation pressure contours. (a) 20% gap, (b) 35% gap, (c) 50% gap.

8

Figure 5. Second-stage-stator time-average pressure contours. (a) 20% gap, (b) 35% gap, (c) 50% gap.

Figure 6. Second-stage-stator standard-deviation pressure contours. (a) 20% gap, (b) 35% gap, (c) 50% gap.

9

Figure 7. Pressure amplitude. (a) 20% gap, (b) 35% gap, (c) 50% gap.

10
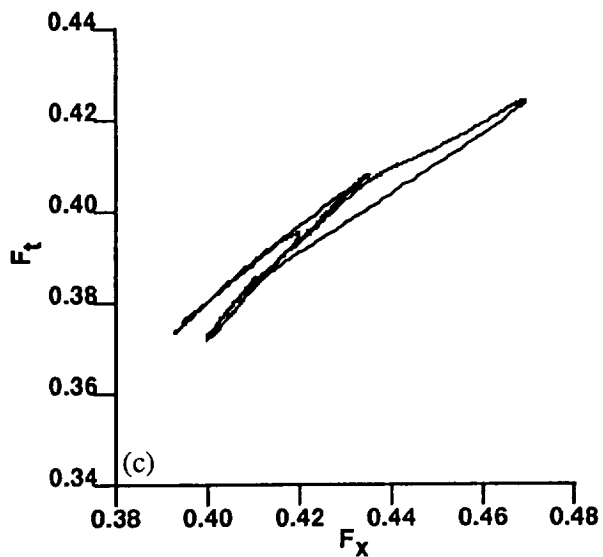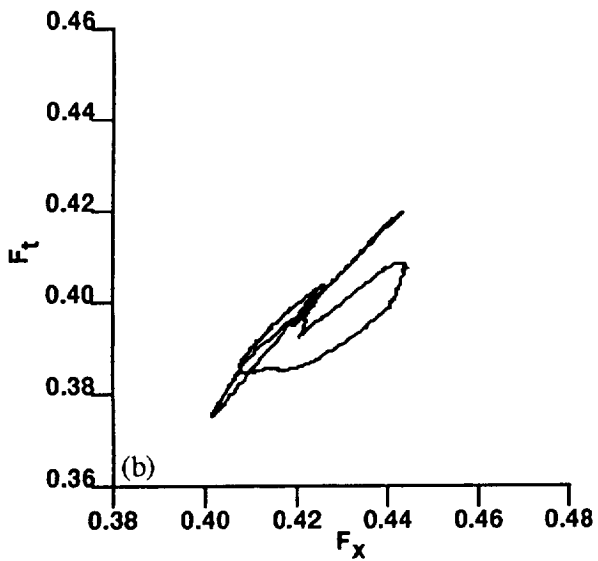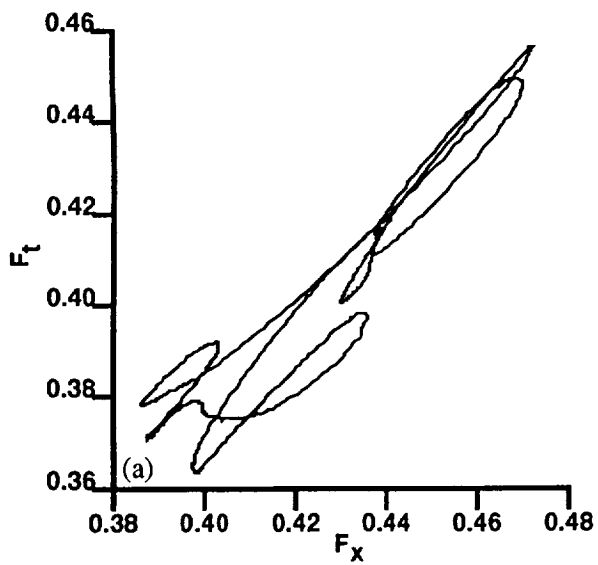
Figure 8. Second-stage-rotor force polars. (a) 20% gap, (b) 35% gap, (c) 50% gap.
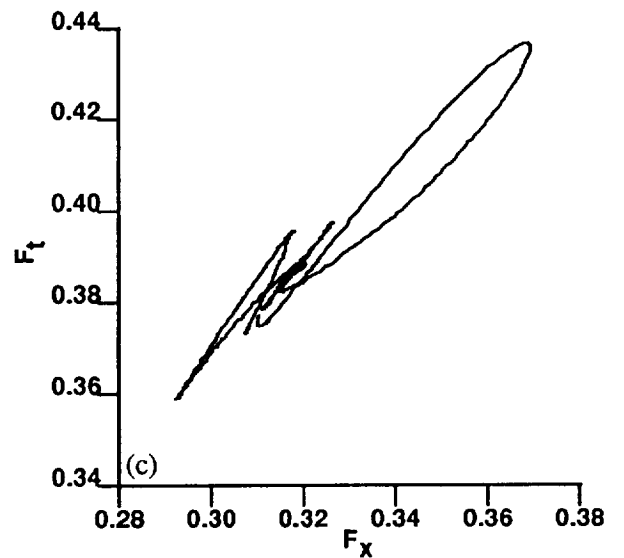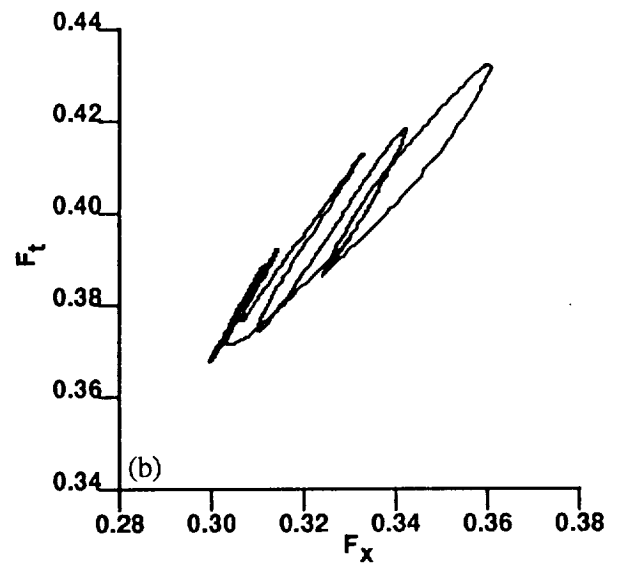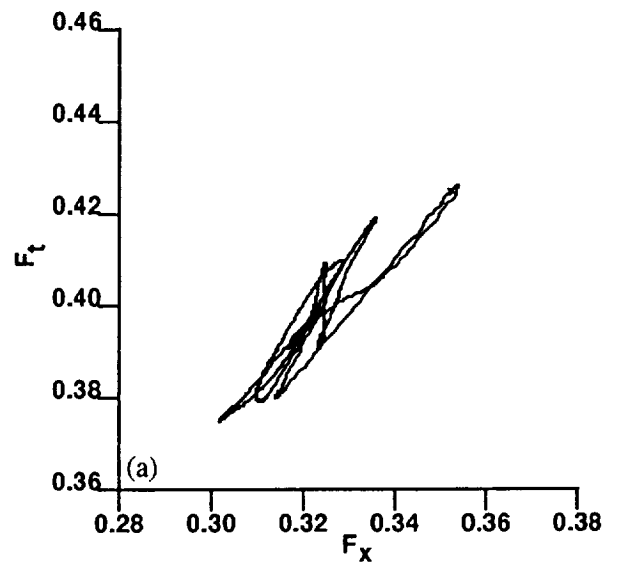
Figure 9. Second-stage-stator force polars. (a) 20% gap, (b) 35% gap, (c) 50% gap.

REPORT DOCUMENTATION PAGE

1. AGENCY USE ONLY *(Leave blank)*	2. REPORT DATE	3. REPORT TYPE AND DATES COVERED
	June 1992	Technical Memorandum

4. TITLE AND SUBTITLE

Computations of Unsteady Multistage Compressor Flows
in a Workstation Environment

5. FUNDING NUMBERS

505-60

6. AUTHOR(S)

Karen L. Gundy-Burlet

7. PERFORMING ORGANIZATION NAME(S) AND ADDRESS(ES)

Ames Research Center
Moffett Field, CA 94035-1000

8. PERFORMING ORGANIZATION REPORT NUMBER

A-91074

9. SPONSORING/MONITORING AGENCY NAME(S) AND ADDRESS(ES)

National Aeronautics and Space Administration
Washington, DC 20546-0001

10. SPONSORING/MONITORING AGENCY REPORT NUMBER

NASA TM-103839

11. SUPPLEMENTARY NOTES

Point of Contact: Karen L. Gundy-Burlet, Ames Research Center, MS 258-1, Moffett Field, CA 94035-1000
(415) 604-4475 or FTS 464-4475

12a. DISTRIBUTION/AVAILABILITY STATEMENT

Unclassified — Unlimited
Subject Category 07

12b. DISTRIBUTION CODE

13. ABSTRACT *(Maximum 200 words)*

High-end graphics workstations are becoming a necessary tool in the computational fluid dynamics environment. In addition to their graphics capabilities, workstations of the latest generation have powerful floating-point-operation capabilities. As workstations become common, they could provide valuable computing time for such applications as turbomachinery flow calculations. This report discusses the issues involved in implementing an unsteady, viscous multistage-turbomachinery code (STAGE-2) on workstations. It then describes work in which the workstation version of STAGE-2 was used to study the effects of axial-gap spacing on the time-averaged and unsteady flow within a 2 1/2-stage compressor. The results include time-averaged surface pressures, time-averaged pressure contours, standard deviation of pressure contours, pressure amplitudes, and force polar plots.

14. SUBJECT TERMS

Multistage turbo machinery, CFD, Workstation computing

15. NUMBER OF PAGES

14

16. PRICE CODE

A02

17. SECURITY CLASSIFICATION OF REPORT	18. SECURITY CLASSIFICATION OF THIS PAGE	19. SECURITY CLASSIFICATION OF ABSTRACT	20. LIMITATION OF ABSTRACT
Unclassified	Unclassified		